Numerical analysis of methane/oxygen laser ignition in a subscale combustion chamber: flame development in simulation and experiment

M. Wohlhüter[⋆†] *and V. P. Zhukov*[⋆⋆]

DLR Lampoldshausen, Institute of Rocket Propulsion
Langer Grund, 74239 Hardthausen am Kocher, Germany

[⋆]*Michael.Wohlhueter@dlr.de*
[⋆⋆]*Victor.Zhukov@dlr.de*

[†]Corresponding author

Abstract

Numerical investigations of the ignition of methane/oxygen in an experimental 400 N thruster have been done, employing four different combustion models. Two of them use reduced, global kinetic reaction mechanisms, while the other two depend on laminar flamelet formulations. Qualitative comparison of the cold flow before ignition in experiment and simulation is done before analyzing the flame development in experiment and simulations and evaluating the performance of the combustion models. While modeling of the cold flow is qualitatively accurate, the combustion models are unable to capture the flame acceleration and thus the pressure peak observed in the experiment.

1. Introduction

Up to now methane has never been used as rocket fuel in a flight mission, but interest in usage of this combination as rocket propellant increased in the recent years. For upper stage engines and long duration scientific missions it can provide beneficial properties compared to the commonly used fuels. Reliable ignition is crucial for the usage of a rocket engine, especially for mission scenarios requiring ignitions at space conditions. Thus, in order to use methane as rocket fuel detailed knowledge about the flame behavior in methane/oxygen mixtures inside rocket combustion chambers is essential.
Experimentally ignition has been under investigation for many years, but numerical simulations, especially of the ignition of methane/oxygen mixtures, have not been done in much detail. At DLR Lampoldshausen several experimental investigations of laser ignition in subscale combustion chambers have been done [1, 2], as well as some numerical investigations [3]. Especially regarding rocket combustion chambers, numerical simulations can provide important insight into the situation and phenomena occurring in the combustion chamber, where measurement access is very limited. While in experiments quantitative data is mainly restricted to pressure and temperature measurement at selected points, simulations can provide data of the flow field as well as species and temperature distribution.
In order to be one day able to predict the behavior of a rocket motor it is important to simulate all phenomena occurring in the combustion chamber. Up to now only single aspects have been considered at a time, so for example ignition, the heat flux to the wall or flow behavior in a cooling channel. Phenomena like combustion instabilities are usually not only connected to one specific part of the rocket engine, but coupled to several parts interacting with each other. One aspect with the capability to trigger combustion instabilities is a hard ignition with a strong pressure peak. To be able to get information of the overall performance of a combustion chamber it would be preferable to combine all those phenomena in one large simulation. To do this, the single parts have to work efficiently with as low computational requirements as possible. Thus investigations with reduced, time efficient reaction mechanisms are done.
The experiment can be divided in two parts: The first part is the cold flow before ignition, the second part includes the energy deposition by a laser pulse with subsequent flame development. In the first part the main aspect is the development of the flow field, the mixing of the fuels and their distribution in the combustion chamber. The amount and

distribution of the fuels is connected directly to flame spreading and the pressure peak occurring during ignition. The second part covers the laser pulse and subsequent flame development throughout the combustion chamber. Different regimes can be identified in the process of flame development. First regime is the laminar flame kernel, which develops into a turbulent flame, where in the second regime acceleration of the flame front can occur up to detonation-like flame speeds. Capturing the flame speed in the simulations accurately is important to be able to predict the ignition pressure peak.
Goal of this work is to simulate the transient ignition process of methane/oxygen and interpret the data with focus on the flame development in simulation and experiment.

2. Experimental Setup

For the experimental investigation providing the data used in this work a 400 N experimental thruster and a tabletop laser ignition system was used. The sections below further describe the thruster, the laser ignition system and the measurement systems. This is just a brief overview, more detailed information about the experimental setup can be found in [2, 3].

2.1 The experimental thruster

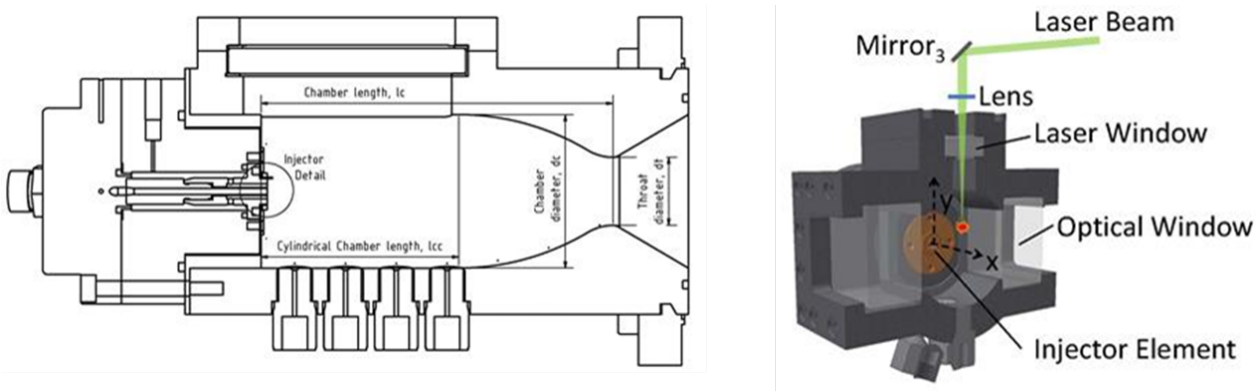

Figure 1: Left: Combustion chamber cross section; Right: Laser path into the combustion chamber

The experimental thruster used for testing is a semi-cylindrical 60 *mm*-diameter combustion chamber. A simple coaxial injector element without recess and tapering is used to inject the propellants into the combustion chamber. The cross section of the combustion chamber is shown in Figure 1, left. Quartz windows in the side walls provide optical access into the chamber, the laser enters through a small window at the top of the chamber, as seen in Figure 1, right.

2.2 The laser ignition system

A frequency doubled tabletop Nd-YAG solid state laser with a wavelength of 532 *nm* was used to deliver the laser pulse for ignition. The power of the laser pulse was in range of 0.09 J. The laser beam was led with a mirror system and focused into the combustion chamber via a lens through the small top window, as seen in Figure 1, right.

2.3 Measurement systems

The combustion chamber is equipped with four dynamic and four static pressure sensors along the lower cylindrical section. These sensors were implemented to measure the ignition pressure peaks and the steady state chamber pressure respectively. The dynamic pressure sensors are piezoelectric sensors while the static pressure sensors are piezoresistive absolute pressure sensors. Dynamic and static pressure sensors are also installed in the injector head to measure the pressure of the propellants in each respective injector dome. Temperature is measured in the injector domes as well as at the combustion chamber walls.
To gather information about the flow conditions and the flame development in the combustion chamber, the testbench is equipped with Schlieren- and OH-/CH-imaging camera systems. A standard Z-setup, as shown in Figure 2, is used for Schlieren imaging. Spontaneous CH*-emission is recorded by an intensified high-speed CCD video camera.

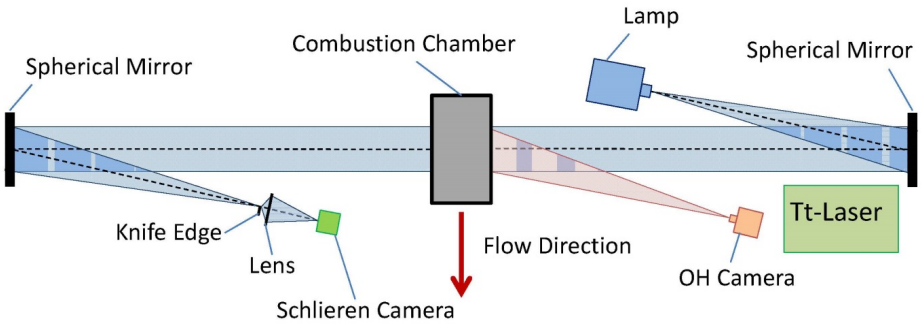

Figure 2: Optical diagnostics setup

3. Ignition simulation

The simulations were done with the commercial CFD solver ANSYS CFX, version 14.5 [4]. The Shear Stress Turbulence (SST)-model of Menter [5] was used in the URANS calculations presented in this paper.

3.1 Mesh

The computational domain used in the simulations is composed by three parts:

- Coaxial injector with central oxygen post and surrounding methane annulus
- Combustion chamber with exit nozzle
- Ambient area, into which the combustion gases expand

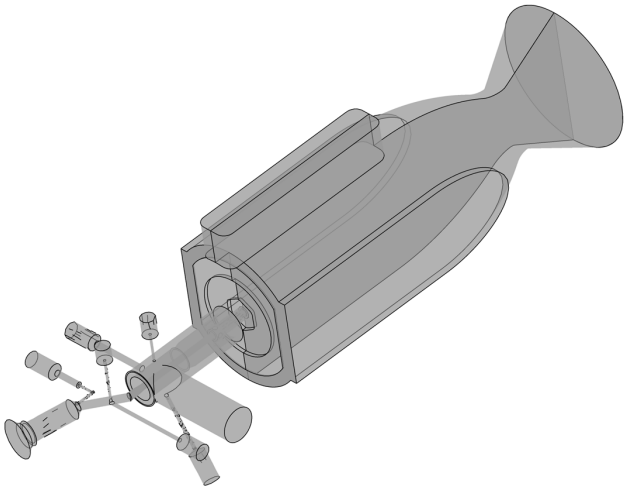

Figure 3: Full 3D-geometry of injector and combustion chamber

As there is no common symmetry plane for the combustion chamber and the injector geometry, only simulations taking into account the full 3D geometry can produce all effects caused by the flow. Previous investigations have shown that simplifications made to reduce the mesh size such as reorientation of the injector to match the symmetry planes and model a 180°-geometry influence the distribution of propellants in the combustion chamber and thus the ignition process [3]. Figure 3 shows the geometry of the combustion chamber and the injector geometry in their appropriate orientation. The combustion chamber mesh consists of 1.2 Mio nodes, the injector mesh of 150000 nodes.

3.2 Initialisation and boundary conditions

Preceding each test the combustion chamber is purged with nitrogen to ensure defined start conditions. Hence, as initial condition of the simulation the combustion chamber and the injector are completely filled with quiescent nitrogen at

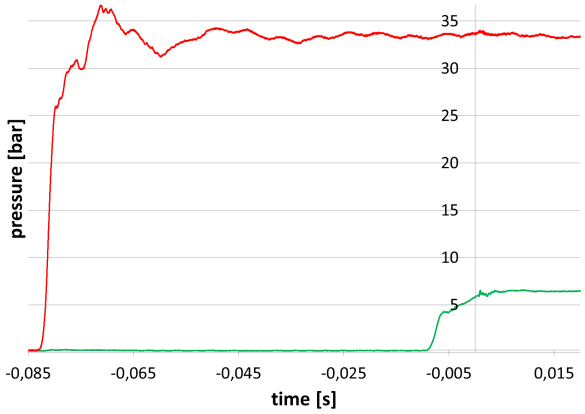

Figure 4: Injector dome pressures; green: Methane dome; red: Oxygen dome

ambient conditions. The ambient area is defined as air at ambient conditions. The simulation starts with the opening of the oxygen valve, covers the pressure rise in the injector domes, the filling of the combustion chamber with propellants and subsequently the laser pulse and flame development with the pressure peak following the laser ignition and the relaxation of the combustion chamber pressure to the steady state value. In total approximately 0.1 s of the experiment are calculated.
All walls of the injector are treated as adiabatic walls, in the combustion chamber they are defined as isothermal walls at ambient temperature. During ignition this is a valid assumption, as there is not enough time for the flame to heat up the walls. The no-slip-condition is applied to all walls. At the outlet boundary of the ambient area fluid can leave and enter the numerical domain. The fluid entering is air at ambient conditions. Massflow is specified as inlet-condition for both the oxygen and methane inlet. Therefore the massflow measured in steady state conditions towards the end of the experiment is normalized by the pressure level in the injector domes, which are shown in the graph in Figure 4, to achieve the proper mass flow development in time. Here the assumption is that mass flow through the injector is proportional to the pressure level in the injector dome. Methane and oxygen both have the temperature of $T = 278\ K$. The massflows of the fully developed flow are $\dot{m}_{CH4} = 12.23\ g/s$ and $\dot{m}_{O2} = 37.25\ g/s$.

3.3 Combustion simulation

Four different combustion models have been used to model the flame development in the combustion chamber. The first two methods use different global, reduced kinetic reaction mechanisms, the other two are based on laminar flamelet models.

1. Global, reduced 2-step reaction mechanism of Westbrook and Dryer [6] with the Water Gas Shift reaction together with the combined Finite Rate Chemistry/Eddy Dissipation combustion model (FRC/EDM). Results of this calculation are marked with "2step".

2. Global, reduced 2-step reaction mechanism of Westbrook and Dryer [6] with the Water Gas Shift reaction together with the Finite Rate Chemistry combustion model (FRC). Results of this calculation are marked with "2step FRC".

3. Global, reduced 4-step reaction mechanism of Jones and Lindstedt [7] together with the Finite Rate Chemistry combustion model (FRC). Results of this calculation are marked with "4step".

4. Extended Coherent Flame Model (ECFM). Laminar flamelet with PDF is used as model for the composition of the reacted and nonreacted fractions of the fluid, while for calculation of the turbulent burning velocity an additional transport equation for the flame surface density is introduced [8]. Results of this calculation are marked with "ECFM".

5. Burning Velocity Model (BVM). The Burning Velocity Model, or also called Turbulent Flame Closure, is also based on the Laminar Flamelet formulation, but in contrast to ECFM uses an algebraic correlation for modeling the turbulent burning velocity [8]. Results of this calculation are marked with "BVM".

FRC uses the assumption of slow chemistry, the chemical reaction processes define the progress of the combustion. In contrast to this EDM assumes fast chemical reactions, so the progress of the combustion is limited by mixing processes

of the propellants or hot and cold gases [9]. The combined model FRC/EDM aims to cover both regimes by calculating the reaction rates for both models and using the lower value, thus employing the limiting model for each step.
Flamelet formulation allows to incorporate several intermediate species in the calculation without slowing down the calculation considerably, as no transport equations have to be solved for them. With ECFM and BVM the species are not calculated directly during the calculation, but a reaction progress variable is used to mark the progress of the combustion and the species values are computed from flamelet libraries.

4. Results

4.1 Cold flow

The amount and distribution of propellants in the combustion chamber define the flame development during the ignition process and the pressure peak resulting from the combustion energy release. In the experiments the ignition pulse was triggered already 7 ms after opening the methane valve, as shown in Figure 4. Ignition takes place at $t_{ign} = 0\ s$. This test sequence was chosen to limit the amount of methane in the combustion chamber at time of ignition in order to prevent hard ignition with a strong pressure peak.

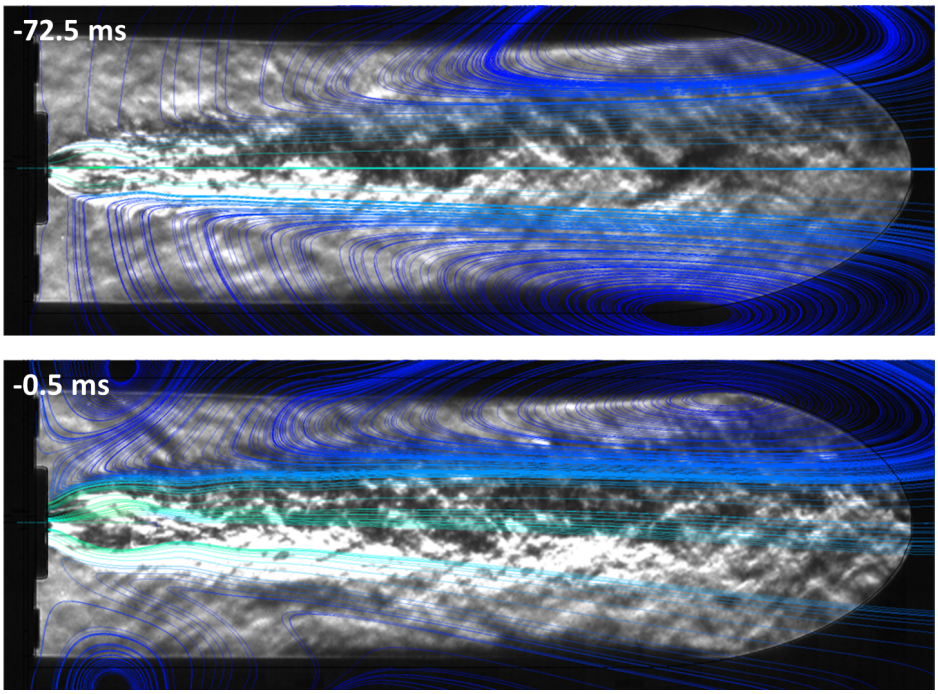

Figure 5: Superposition of experimental Schlieren images and numerical streamlines on the central XY-plane at 72.5 and 0.5 ms before ignition

There is no quantitative measurement of the flow conditions inside the combustion chamber, but a characteristic feature of the flow is the high velocity of oxygen at the inlet of the injector into the combustion chamber. The flow here reaches extensive supersonic velocities and forms a strong barrel flow. This flow characteristic can be used to obtain at least qualitative comparison between experiment and simulations. Figure 5 shows the Schlieren images at 72.5 and 0.5 ms before ignition, superimposed with streamlines from the simulation on the central XY-plane at the respective times. At $-72.5\ ms$ the methane valve is still closed and the oxygen flow is developing, while at $-0.5\ ms$, short before ignition takes place, both the oxygen and methane valves are open. The Schlieren images and streamlines match well for both points in time. The simulation is able to catch the barrel flow as well as the opening angle of the following turbulent main flow accurately. Thus can be said that qualitatively the flow is modeled correctly and with it the distribution of fuels in the combustion chamber at time of ignition is accurate.

4.2 Flame development

One important aspect of the ignition process in regard to operating a rocket engine is the pressure development. Aim is to achieve a soft ignition, to keep the ignition pressure peak as low as possible to avoid damaging the combustion chamber or triggering combustion instabilities. The pressure development is dependent on the energy release of the combustion processes and thus is directly connected with the flame development in the combustion chamber.

4.2.1 Flame development in the experiment

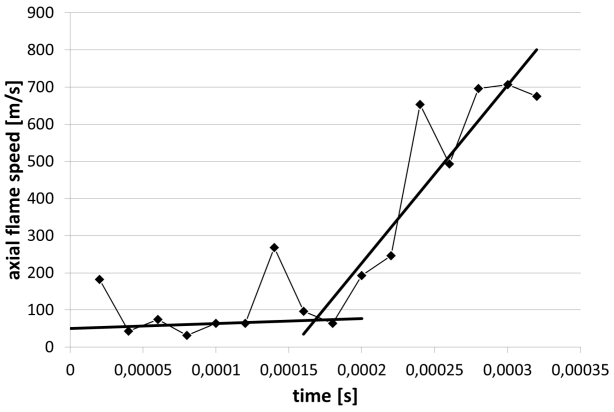

Figure 6: Axial flame speed in the experiment, values and trend lines

There is no quantitative measurement of the flame structure available in the ignition experiments, so direct comparison between experiment and simulation is difficult. However, in the Schlieren images the development of the flame in axial direction is visible up to certain extent. Analyzing these images, the growth of the flame was evaluated by measuring the progression of the leading edge of the flame in axial direction from frame to frame. The pixel-length conversion was achieved by known dimensions like window size and visible faceplate features. The framerate of the Schlieren video was 50000 fps, so one velocity value can be gained every 0.02 ms, up to a time of 0.32 ms after ignition. At this time the flame front moves out of the window and reference point is lost.
Data gained by this is shown in the graph in Figure 6. The calculated velocities are marked with diamonds. The flame development in the experiment can be divided in two phases, as marked with the two solid trend lines in the graph. The first phase is the growth of the flame kernel with the turbulent flame speed, still largely unperturbed by the fast main flow until about 0.18 ms after ignition. From this time on we observe a strong increase in the axial velocity of the flame leading edge towards supersonic speeds and thus a transition from deflagration to detonation. This phenomenon has been identified in [3] as driving phenomenon for the pressure development and level of the ignition pressure peak.

4.2.2 Flame development in the simulations

To gain insight into the behavior of combustion models at ignition simulations and different options to simulate the flame development after the ignition, simulations have been done with four different combustion models. The flame development in the simulations has been analyzed according to the experiment. As "leading edge" of the flame an isosurface at the temperature of $T = 900\ K$ has been defined. This temperature is the ignition temperature of methane/oxygen mixtures and in the simulations the minimum reaction temperature. For the combustion models using kinetic mechanisms the reaction rates are set to zero below this temperature to prevent reactions at low temperatures and too high energy release.
The simulation results in terms of flame development are shown in Figure 7 a-e. In each of the graphs the axial flame speed values are shown along with a trendline to emphasize the temporal development. For comparison in each graph also the experimental values are shown.
The 2step-calculation results in Figure 7a are marked with squares, the corresponding trendline is dash-dotted. The flame speed in the simulation stays constant during large amounts of time at a value of around 170 m/s, which for the first part is significantly higher than the experimental value, while in the second part no flame acceleration is apparent and thus the flame in the experiment grows faster.
Using the pure Finite Rate Chemistry model the calculation with the two step reaction mechanism shows significantly

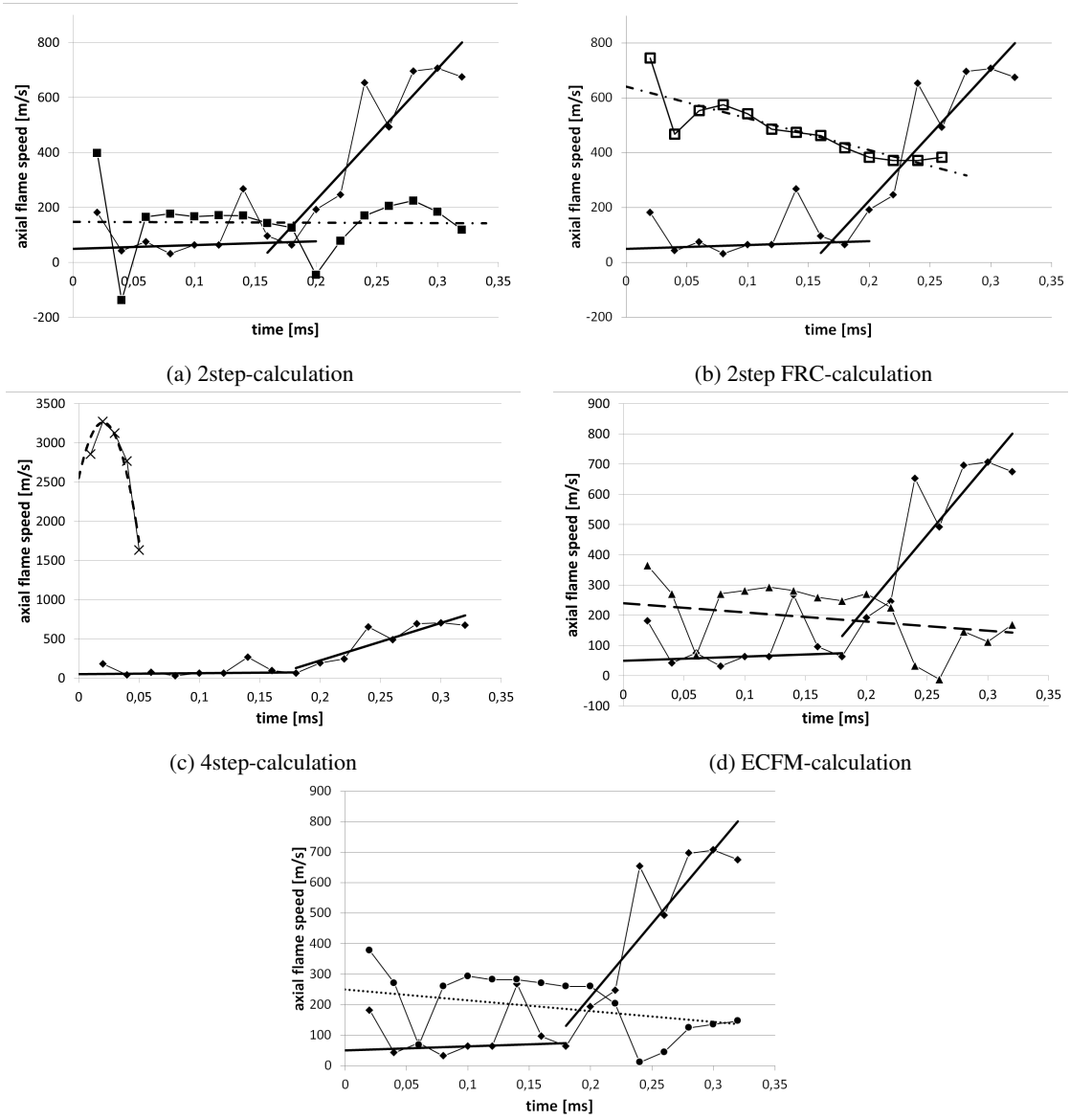

(a) 2step-calculation

(b) 2step FRC-calculation

(c) 4step-calculation

(d) ECFM-calculation

(e) BVM-calculation

Figure 7: Axial flame speed in experiment and simulations

higher flame speeds, results are shown in 7b. The simulation results are marked with the empty squares, with a dashed-double-dotted trendline. The flame speed is with 500 m/s higher than in the previous calculation and decelerates over time, the opposite behavior than what was seen in the experiment.
The results of the 4step-calculation are shown in Figure 7c. The flame speed values are marked with crosses with a short-dashed trendline. The flame velocities in this calculation are in the range of 2000 - 3000 m/s and more than a magnitude higher than those observed in the experiment. The flame is spreading so rapidly in the combustion chamber that only few values could be derived.
The two flamelet formulations in Figure 7d and 7e show very similar behavior to each other. The results of the ECFM-calculation are set with triangles with long-dashed trendline, those of the BVM-calculation with dots and dotted trendline. The axial flame speed level in the range of 290 m/s in the first part is higher than in the 2step-calculation, and the overall development shows a deceleration of the axial flame front, contrary to the observations made in the experiment.
In summary none of the combustion models was able to reproduce the flame behavior observed in the experiment accurately. The flame speeds are too high in the first part and the simulations don't capture the flame acceleration in the second part. Extensive research is done focusing on the phenomenon of Deflagration to Detonation Transition (DDT)

of flames. To capture this transition from deflagration to detonation in simulations, a separate combustion model is required [10]. This has not been used up to now, but will be introduced in the future.

4.3 Pressure development

As mentioned before, the development of the flame and the energy release in this process is the driving mechanism for the pressure development in the combustion chamber. Figure 8 shows the pressure development over time after the ignition pulse at $t_{ign} = 0\ s$. Experimental data is drawn in black. The solid line shows data from the dynamic pressure sensor. Due to its setup as piezoelectric sensor and the flash mounted position directly at the inner combustion chamber wall this type of sensor is sensitive to thermal shock. When the flame has grown sufficiently to heat up the membrane, the sensor loses the pressure signal. Thus data of this sensor is shown only until its maximum value. This maximum value is not necessarily the absolute pressure peak value, but the data shows the pressure development after the ignition pulse with a moderate rise in the first part and a steep pressure rise in the second part, which was expected according to the flame development shown in the previous section.

The dotted line shows the response of the static pressure sensor. This piezoresistive sensor is unable to follow the

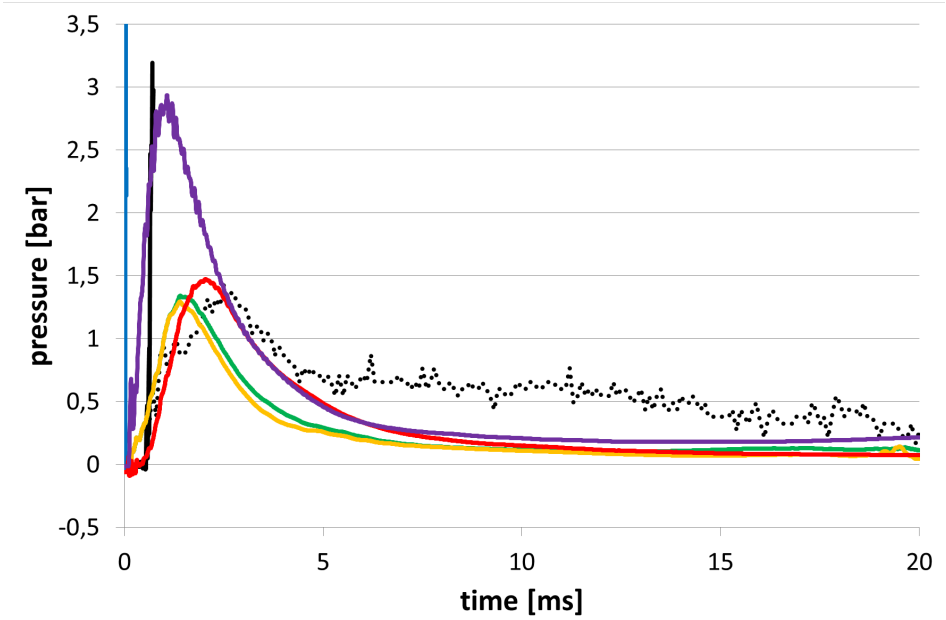

Figure 8: Pressure development; solid black: experimental, dynamic sensor; dotted black: experimental, static sensor; red: 2step-calculation; purple: 2step FRC-calculation; green: ECFM-calculation; yellow: BVM-calculation

steep pressure rise after ignition and shows significantly lower values in this part, but it can provide data in the later part of the experiment, when the pressure moves towards steady state values and data of the dynamic pressure sensor is not reliable any more, as described above.

Numerical data is shown with coloured, solid lines. In red the pressure development in the 2step-calculation is shown. Consistent with the flame development in the first part the pressure rises faster than the experimental chamber pressure, but in further development the pressure rise is less steep and the subsequent pressure peak with $p_{p,2step} = 1.5\ bar$ relative pressure is significantly lower than the maximum dynamic pressure sensor value with $p_{dyn} \geq 3\ bar$. The inclination of the falling pressure after the peak matches the inclination of the static sensor data. As in this interval the pressure drop because of flow condition outweighs the energy release by the combustion model, the pressure drop is modeled appropriately, though in the simulation the steady state pressure is reached faster than in the experiments.

The purple line marks the pressure development in the 2step FRC-calculation. Consistent with the high flame speeds seen above also the pressure rise is much steeper than those of the other calculations. In the first part the pressure rises much faster than what was measured in the experiments, but in the second part doesn't match the rise in the experiment. Also, while the pressure peak with $p_p = 3\ bar$ relative pressure is significantly higher than those of the other calculations, it is still lower than the maximum pressure measured by the dynamic sensor. In the region of pressure relaxation after the pressure peak the gradient matches that of the 2step-calculation and as well that of the static pressure sensor measurement.

The pressure data of the ECFM- and the BVM-calculation are shown in green and yellow lines. As expected due to

the higher axial flame speed, also the pressure increase is faster than in the 2step-calculation, but less steep than in the experiment. Both calculations show similar results up to the pressure peak, with only a slight difference further on. The pressure peak is reached $\Delta t = 0.6\ ms$ earlier than in the 2step-calculation and is $\Delta p = 0.15\ bar$ lower, which presumably is due to the lower amount of methane present at this time. Investigations on the effect of small changes in the time of ignition in [3] showed that a shift to $\Delta t = 0.5\ ms$ later leads to the same rise of peak pressure.
In Figure 8 the results of the 4step-calculation are not shown, because due to the very high flame speed also the pressure increase occurs rapidly and leads to a very high peak pressure value of $p_{p,4step} = 11\ bar$ at a time of $t = 2.4 * 10^{-5}\ s$ after ignition.
The evolution of the flame in time defines the energy release and thus the increase of pressure during the ignition process. To be able to obtain the pressure development in simulations, the flame development and especially the flame acceleration in the second part has to be captured. Phenomena, where flow processes dominate the behavior instead of combustion processes, like the pressure relaxation after the peak pressure, are modeled well, as was also seen in the cold flow section before.

4.4 FRC/EDM vs. FRC

Figure 8 shows the difference in the results of the 2step-FRC/EDM and the 2step-FRC-calculation. The 2step-FRC-calculation shows a steeper pressure increase and a higher pressure peak consistent with the faster flame growth and thus higher energy release than was observed for the 2step-FRC/EDM-calculation. As described in the theory part, the combined model limits the chemical reaction by employing the lower reaction rate of the two models, obviously to a too high extent for this ignition simulation. The FRC on the other hand suffers from the fact that reduced kinetic reaction mechanisms tend to overshoot the energy release by employing too fast reactions. After the pressure peak the pressure value drops at a gradient similar to the FRC/EDM calculation and reaches similar values, which, as said above, correspond well with the static pressure sensor values in that part.

4.5 Computational requirements of the simulations

Table 1: Impact of combustion models on computational requirements

	CPU time per timestep [s]	CPU time for hot flow (0.02 s) [s]
2step	1.70×10^3	$6.88e7$
2step FRC	20.46×10^3	$26.08e7$
4step	60.10×10^3	-
ECFM	2.12×10^3	$5.47e7$
BVM	1.84×10^3	$4.91e7$

In regard to an efficient simulation the time requirements induced by the computational needs of the different combustion models have to be taken into account. Table 1 shows two values: an average CPU time per timestep and the CPU time needed to compute the hot flow up to 0.02 s after ignition. CPU time is the summarized amount of time the CPU needed to perform the calculation. Calculations were done on a DELL Poweredge R815 with four 12-core AMD Opteron 6174 CPUs.
The averaged timestep value has been calculated by averaging the CPU time needed for 500 timesteps with the timestep length $\Delta t = 10^{-8} s$. This evaluation focuses on timesteps, not the single iterations, because the duration of a transient simulation is defined by the amount of timesteps or a predefined simulated time. Depending on the complexity of the simulation one timestep needs different amount of iterations to reach the convergence criteria. Table 1 shows that as with the very similar results, also in terms of computational needs the two flamelet-formulations ECFM and BVM behave very similar, with BVM having a slightly lower demand. The 2step-calculation is even quicker, while the two calculations with the Finite Rate Chemistry model show significantly higher values. The CPU time per timestep needed by the 2step FRC-calculation is ten times higher than that of the three calculations mentioned before, the 4step calculation shows a CPU time per timestep which is 30 times higher than the first three and three times higher than that of the 2step FRC-calculation. This is because of the additional set of equations for the combustion model and the species which have to be solved for each iterations, together with the increased complexity and thus more problems with convergence. This increase of computational needs has to be taken into account when thinking about introducing more detailed kinetic reaction mechanisms in the future.
The second value is the CPU time needed to calculate a physical time of 0.02 s of the hot flow, beginning with the ignition pulse. This value takes into account different settings of timestep evolution in course of the calculation. These

different settings were necessary to ensure the stability of the calculation. The results show similar CPU requirements for the calculations using the flamelet model, as was also seen in the average CPU time per timestep. The 2step-calculation on the other hand shows a slightly higher CPU time than the other two models. Due to stability reasons smaller timesteps were necessary, thus a bigger number of timesteps had to be calculated to reach the physical time length and higher CPU time ensued. The difference to the 2step FRC-calculation is less than seen for the single timestep, the overall CPU time needed in that calculation is increased by a factor of five compared to the three calculations mentioned before. No value is shown for the 4step-calculation, as this calculation had to be stopped before reaching a physical time of 0.02 s.

5. Summary

Numerical investigations of the ignition of methane/oxygen in an experimental 400 N thruster have been done, employing different combustion models. Three of them use reduced, global kinetic reaction mechanisms, while the other two depend on laminar flamelet formulations.
In a first step the Cold Flow before ignition has been analysed and a qualitative comparison of the flow fields in experiment and simulation has been done. The numerical streamlines match the phenomena visible in the Schlieren images as well in early stages of the experiment and also short before ignition takes place. Qualitatively the flow development before ignition is captured and with it the distribution of propellants to set the conditions for ignition.
The flame development in the experiment was investigated by evaluating the progression of the leading edge of the flame seen in the Schlieren images in X-direction. This axial flame speed development over time can be divided in two parts. In the first part the flame kernel grows as turbulent flame with constant axial flame speed until a certain size, after which the flame front is accelerated towards supersonic speeds and a transition from deflagration to detonation ensues. This flame evolution defines the pressure development during the ignition process with a slow pressure rise in the first instances and a steep increase later on. The simulations were not able to capture this flame behavior. The calculations show too high flame velocities in the first part of flame development to a different extent, but don't capture flame acceleration. The axial flame speed in the simulations retains a constant value or shows a deceleration over time, so that in the second part the flame growth is slower than in the experiment. In consequence of that the combustion chamber pressure in the first instant rises faster than in the experiment, but in the further development the pressure in the experiment grows considerably stronger and leads to higher peak pressures. After the pressure peak the pressure drop in the combustion chamber is captured appropriately, because the flow conditions outweigh the energy release by the combustion model. The 4step-calculation shows very high axial flame velocities from the first instant, resulting in a very strong pressure rise and high pressure peak.
The comparison of the computational requirements shows that the average CPU time per timestep of the 2step-, ECFM- and BVM-calculations were in the same range, while the requirements of the calculations with the Finite Rate Chemistry model were significantly higher. The 2step FRC-calculation the CPU time per timestep was ten times higher than that of the three calculations mentioned before, the requirements of the 4step-calculation were 30 times higher. This increase in CPU time has to be taken into account when employing more detailed kinetic reaction mechanisms.
In conclusion the flame acceleration in the second part of flame development is the main factor defining the pressure profile and level of the ignition pressure peak. To be able to obtain the pressure development in simulations, the flame development and especially the flame acceleration in the second part has to be captured. Characteristics, where flow processes dominate the behavior instead of combustion processes, like the flow development in the cold flow before ignition and the pressure relaxation after the pressure peak, are modeled well. As next steps further investigations regarding the processes leading to the flame acceleration both in experiment and simulation will be done in order to increase understanding of the ignition process and enable the prediction of the ignition pressure peak.

Acknowledgment

We want to thank Chiara Manfletti and Michael Börner for sharing their experimental expertise with us in fruitful discussions about the phenomena occurring in the experiments and interpreting the results.

References

[1] Pauly, C., Sender, J., and Oschwald, M. Ignition of a Gaseous Methane/Oxygen Coaxial Jet. In *2nd European Conference for Aerospace Sciences (EUCASS)*, 2007.

[2] Manfletti, C. and Börner, M. Ignition Overpressure in Laser Ignited Reaction and Control Thrusters. In *50th AIAA/ASME/SAE/ASEE Joint Propulsion Conference*, Cleveland, OH, USA, July 2014.

[3] Wohlhüter, M., Zhukov, V. P. and Manfletti, C. Numerical Analysis of Laser Ignition and Flame Development in a Subscale Combustion Chamber. In *Space Propulsion Conference*, 2014

[4] ANSYS® ANSYS CFX Academic Research, Release 14.5, 2013

[5] Menter, F. R. Two-Equation Eddy-Viscosity Turbulence Models for Engineering Applications. In *AIAA Journal*, August 1994

[6] Westbrook, C. K. and Dryer, F. L. Simplified Reaction Mechanisms for the Oxidation of Hydrocarbon Fuels in Flames. In *Combustion Science and Technology, Vol. 27*, pages 31-43, 1981

[7] Jones, W. P. and Lindstedt, R. P. Global reaction schemes for hydrocarbon combustion. In *Combustion and Flame, Vol. 73, No. 3*, pages 233-249, September 1988

[8] ANSYS® ANSYS Academic Research, Release 14.5, Help System, ANSYS CFX-Solver Theory Guide, 2013

[9] Magnussen, B. F., Hjertager, B. H. On mathematical modeling of turbulent combustion with special emphasis on soot formation and combustion. In *Proc. 16th Int. Symp. on Combustion, The Combustion Institute, Pittsburgh, PA*, 1976

[10] Kessler, D. A., Gamezo, V. N. and Oran, E. S. Simulations of flame acceleration and deflagration-to-detonation transitions in methane-air systems. In *Combustion and Flame, Vol. 157*, pages 2063-2077, 2010